ELSEVIER

Journal of Power Sources 114 (2003) 80–87

JOURNAL OF POWER SOURCES

www.elsevier.com/locate/jpowsour

Discharge characteristics of planar stack fuel cells

Y. Shiratori*, Y. Yamazaki

Department of Innovative and Engineered Materials, Tokyo Institute of Technology, 4259 Nagatsuta-cho, Midori-ku, Yokohama 226-8502, Japan

Received 15 April 2002; received in revised form 10 September 2002; accepted 26 September 2002

Abstract

A fuel cell system with planar stack configuration is studied with a view of portable applications. A mathematical model to estimate the discharge characteristics of the system is presented in this research to clarify the effect of the number of segmented cells on the output power and energy losses generated in the system. In the isothermal case of this analysis, we revealed that output power of a planar stack SOFC increases with increasing the number of cell segments because the current distribution in the electrolyte becomes more uniform by increasing the number and this results in a reduction of energy losses in the system.

Keywords: Planar stack; Cell partition; Series connection; Mathematical analysis; Energy losses; SOFC

1. Introduction

In the conventional fuel cells, in order to produce a practical output power, there is need for stacking several cells with bipolar separators. The use of separators make the structure of fuel cells very complicated and has been a principal problem in miniaturization of the fuel cells. Recently, we proposed novel small size SOFC called SSSC [1] in which the segmented cells are connected in series and placed in a row in the flow direction of fuel–oxidant mixture without separators. We expect that SSSC (Fig. 1) is easier to produce than that of conventional SOFC stack because of no separator. The stack configuration is called "planar stack" in this research, and in the previous paper [1], we dealt with an analysis of the planar stack SOFC using very simple mathematical model which employs Newman's assumption [2] that the sum of the activation overpotential and concentration overpotential is constant on either electrodes over the whole cell area. The model is very simple and if a load current is given, we can obtain cell voltage without complicated iteration procedure, however the model is not taking *IR* drop in both the electrodes and potential distribution in the electrolyte into consideration and corresponding to the hypothetical fuel cell modeling when the electrode resistances are 0. Discharge characteristics of SOFC are strongly affected by not only operating conditions such as cell current, temperature and partial pressures but also structural parameters such as thicknesses and lengths of electrode and electrolyte. Structural parameters are closely related to potential distribution in each component material, and the changes of the distributions result in output power change. Therefore, for the development of the planar stack fuel cell having optimum dimensions, it is important to estimate the influences of structural parameters on the discharge characteristics with more practical calculation model considering potential distribution in each cell component.

In this paper, we are dealing with fuel/oxidant separate system, then fuel–oxidant mixture system is not considered. Our aim is not to analyze the performance of one-chamber fuel cell. The most emphasis on this paper is to quantitatively clarify the effect of the cell partition along gas flow direction through the analysis of the planar stack fuel cells. If the fuel–oxidant mixture, namely the partial oxidation of hydrocarbon is considered, the system will become very complicated. The merit of the cell partition discussed in this paper is expected in all types of fuel cells, that is to say not only in one-chamber fuel cell. Therefore, for the simplification, we discussed only for the fuel/oxidant separate system.

2. Theory

For the single cell schematically shown in Fig. 2, the potential distribution can be considered by the equivalent circuit of Fig. 3. In the SOFC, because the resistivity of the electrolyte is considerably larger than that of electrode,

* Corresponding author.
E-mail address: yusuke_shiratori@hotmail.com (Y. Shiratori).

0378-7753/02/$ – see front matter
PII: S0378-7753(02)00526-8

Nomenclature

d	electrolyte thickness (m)
$E_{\text{loss, act}}$	energy loss caused by activation overpotential (W)
$E_{\text{loss, el}}$	energy loss caused by *IR* drop in the electrodes (W)
$E_{\text{loss, ion}}$	energy loss caused by *IR* drop in the electrolyte (W)
emf	electromotive force (V)
emf*	net electromotive force (V)
F	Faraday constant (C mol^{-1})
$\Delta G^{\circ}(T)$	standard Gibbs energy change at T K (J mol^{-1})
$\Delta H^{\circ}(T)$	standard enthalpy change at T K (J mol^{-1})
I_0	load current (A)
I_a	current in the anode (A)
I_c	current in the cathode (A)
I_e	current in the electrolyte (A m^{-1})
k	rate constant (A m^{-2})
L	cell length (m)
M_i	molar flow rate (mol s^{-1})
n	segment number
N	the number of segment cells
P	total pressure (atm)
P_i	partial pressure (atm)
R	gas constant (J mol^{-1} K^{-1})
R_a	electric resistance of anode (Ω m^{-1})
R_c	electric resistance of cathode (Ω m^{-1})
R_e	electric resistance of electrolyte (Ω m)
t	electrode thickness (m)
T	temperature (K)
U_{H_2}	hydrogen utilization (%)
$V(I_0)$	cell voltage at given cell current (V)
$V_t(I_0)$	total cell voltage of planar stack fuel cell (V)
W	cell width (m)
x	position (m)
X	molar flow rate of oxygen atom in the fuel gas (mol s^{-1})

Greek letters

ε_{th}	theoretical thermal efficiency of fuel cell (%)
$\varepsilon_{\text{con, s}}$	energy conversion efficiency of fuel cell system (%)
$\varepsilon_{\text{con, e}}$	energy conversion efficiency from chemical energy to electricity (%)
η	activation overpotential (V)
η_{IR}	*IR* drop (V)
ρ	resistivity (Ω m)

Subscripts

a	anode
ave	average
c	cathode
e	electrolyte
f	fuel gas mixture
max	maximum
ox	oxidant gas mixture

current is assumed to pass parallel to gas flow direction in the electrodes and normal to in the electrolyte. Nagata et al. have reported some numerical analyses on conventional SOFC characteristics using this model [3–5]. Based on the model, Mathematica™ program that can calculate partial pressure, current and potential distributions and *I–V* (current–voltage) and *I–P* (current–output power) curves of a planar stack SOFC was made in this research.

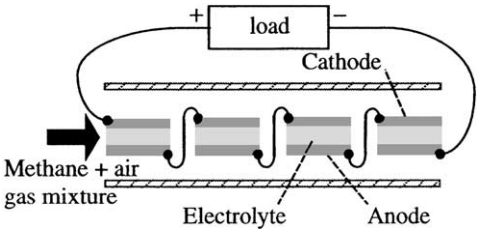

Fig. 1. Schematic diagram of a single chamber SOFC with series connected cells, which is abbreviated to SSSC.

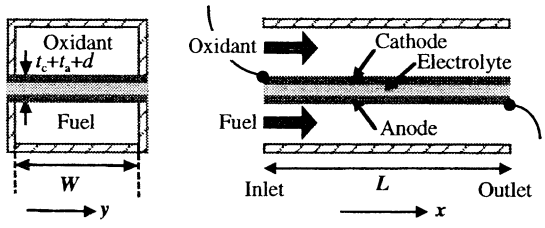

Fig. 2. Single cell configuration.

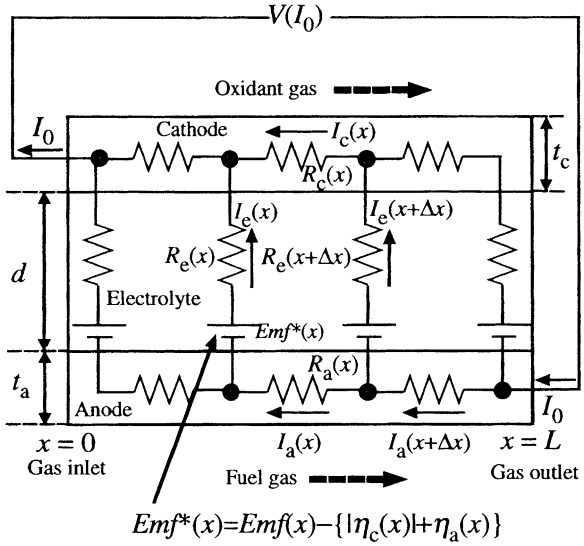

Fig. 3. Equivalent circuit of s planar SOFC.

In order to understand the effect of the cell partition along gas flow direction intrinsically, first of all, discharge characteristics of planar stack fuel cell should be analyzed neglecting heat transfer in the cell. In the case of the analysis, temperature increase in the cell are not taken into consideration, in other words, all heats from the cell caused by *IR* drops, activation overpotentials and reaction entropy are released from the fuel cell system without contribution to temperature increase in the cell. The case of the analysis is referred to as "isothermal case".

2.1. Current distribution

In order to consider the effect of the activation overpotential on the SOFC output power, the net electromotive force, $\mathrm{emf}^*(x)$ is introduced. The $\mathrm{emf}^*(x)$ is expressed as the subtraction of the activation overpotential $\{|\eta_c(x)| + \eta_a(x)\}$ from the electromotive force, $\mathrm{emf}(x)$. By applying the Kirchhoff's law to a small area of x axis in the model, we have following equations:

$$I_e(x) = \frac{dI_a(x)}{dx} \tag{1}$$

$$\frac{d\{I_e(x)\,R_e(x)\}}{dx} = -I_c(x)\,R_c(x) + I_a(x)\,R_a(x) + \frac{d\mathrm{emf}^*(x)}{dx} \tag{2}$$

Eq. (1) means that the difference in current in the anode $I_a(x)$ between $x + \Delta x$ and x is equal to current in the electrolyte $I_e(x)$. Eq. (2) indicates that the current distribution in the electrolyte is controlled by *IR* drop in the cathode and anode and net electromotive force distribution. Moreover, the following relationship holds among $I_a(x)$, $I_c(x)$ and I_0:

$$I_a(x) + I_c(x) = I_0 \tag{3}$$

The differential equation related to current in the anode $I_a(x)$ is derived from Eqs. (1)–(3).

$$\frac{d^2I_a(x)}{dx^2} = -\frac{dI_a(x)}{dx}\frac{dR_e(x)}{dx}\frac{1}{R_e(x)} + I_a(x)\frac{R_c(x) + R_a(x)}{R_e(x)} + \left\{\frac{d\mathrm{emf}^*(x)}{dx} - I_0R_c(x)\right\}\frac{1}{R_e(x)} \tag{4}$$

We can solve this equation by giving initial net electromotive force and some boundary conditions, then the current distributions in the anode $I_a(x)$ can be obtained. When the load current is I_0, $I_a(L) = I_0$ and $I_a(0) = 0$ are the boundary conditions. In this case, $I_a(L) = I_0$ is used to find the value of $(dI_a(x)/dx)_{x=0}$ which is essential for solving differential equation of second order (Eq. (4)). First, Eq. (4) is solved using $I_a(0) = 0$ and temporary value of $(dI_a(x)/dx)_{x=0}$. Next, the value of $(dI_a(x)/dx)_{x=0}$ is changed so that $I_a(L) = I_0$ can be satisfied, and when it is satisfied, we can obtain right solution. Using the solution, current distribution in the cathode $I_c(x)$ and electrolyte $I_e(x)$ can be obtained with Eqs. (1) and (3), respectively.

2.2. Mass balance in oxidant gas mixture

In this paper, SOFC for H_2–O_2 system is considered. Therefore, only oxygen molecule is the reactive species in the oxidant gas mixture. The cathode reaction is expressed by:

$$\tfrac{1}{2}O_2 + 2e^- \rightarrow O^{2-} \tag{5}$$

Hence, oxygen atom transfers across the electrolyte as the form of oxide ion from cathode side to anode side. This transfer is equivalent to the current flow in the electrolyte from anode to cathode. Then, oxygen atom in the oxidant gas mixture is consumed at any position of x by the quantity corresponding to $I_e(x)$. Moreover, according to Eq. (1), current in the anode at x is equal to the integration of current in the electrolyte from 0 to x. Therefore, $I_a(x)$ corresponds to the amount of oxygen moved across the electrolyte from 0 to x. Consequently, the oxygen molar flow rate in the oxidant gas $M_{O_2,\mathrm{ox}}(x)$ gradually decreases in the gas flow direction. This behavior can be expressed by:

$$M_{O_2,\mathrm{ox}}(x) = M_{O_2,\mathrm{ox}}(0) - \frac{I_a(x)}{4F} \tag{6}$$

where $M_{O_2,\mathrm{ox}}(0)$ is oxygen molar flow rate at oxidant gas entrance.

2.3. Mass balance in fuel gas mixture

Hydrogen, water vapor and nitrogen gases are supplied into anode side, therefore in the fuel gas, reactive species are hydrogen, water vapor and oxygen. The anode reaction is expressed by:

$$H_2 + O^{2-} \rightarrow H_2O + 2e^- \tag{7}$$

Molar flow rate of oxygen atom in the fuel gas $X(x)$ is expressed as:

$$X(x) = M_{H_2O,\mathrm{f}}(0) + \frac{I_a(x)}{2F} \tag{8}$$

where $M_{H_2O,\mathrm{f}}(0)$ is molar flow rate of water vapor at fuel inlet.

Thus, in the fuel gas mixture, we can obtain concentration distributions of reactive species $M_{O_2,\mathrm{f}}(x)$, $M_{H_2,\mathrm{f}}(x)$ and $M_{H_2O,\mathrm{f}}(x)$ from the following simultaneous equations [3]:

$$M_{H_2O,\mathrm{f}}(x) + 2M_{O_2,\mathrm{f}}(x) = M_{H_2O,\mathrm{f}}(0) + \frac{I_a(x)}{2F} \tag{9}$$

$$M_{H_2O,\mathrm{f}}(x) + M_{H_2,\mathrm{f}}(x) = M_{H_2O,\mathrm{f}}(0) + M_{H_2,\mathrm{f}}(0) \tag{10}$$

$$\frac{M_{H_2O,\mathrm{f}}(x)}{M_{H_2,\mathrm{f}}(x)\,P_{O_2,\mathrm{f}}(x)^{0.5}} = K \tag{11}$$

Eqs. (9) and (10) indicate mass balances for the oxygen atom and the hydrogen atom, and Eq. (11) indicates mass action law, where $P_{O_2,\mathrm{f}}(x)$ is the partial pressure of oxygen and K the equilibrium constant for the combustion of hydrogen at operating temperature.

2.4. Potential distribution

Partial pressure distribution of component i, $P_i(x)$ is given by:

$$P_i(x) = \frac{M_i}{\sum M_i} P \tag{12}$$

where M is molar flow rate and P the total pressure. In the oxidant gas mixture, components are oxygen and nitrogen, in the fuel gas mixture, hydrogen, water vapor, oxygen and nitrogen.

Distribution of electromotive force can be calculated by:

$$\mathrm{emf}(x) = \frac{RT}{4F} \ln\left\{\frac{P_{\mathrm{O_2,ox}}(x)}{P_{\mathrm{O_2,f}}(x)}\right\} \tag{13}$$

where indices ox and f means oxidant and fuel, respectively.

When the dissociation and adsorption of the reactive species is rate determining step, Butler–Volmer equations for the current in the electrolyte are expressed as following equations [6]:

for the cathode reaction

$$I_e(x) = Wk_c P^{1/4}_{\mathrm{O_2,ox}}(x)\left[\exp\left\{-\frac{F}{RT}\eta_c(x)\right\} - \exp\left\{\frac{F}{RT}\eta_c(x)\right\}\right] \tag{14}$$

for the anode reaction

$$I_e(x) = -Wk_a P^{1/4}_{\mathrm{H_2,f}}(x)\left[\exp\left\{-\frac{F}{RT}\eta_a(x)\right\} - \exp\left\{\frac{F}{RT}\eta_a(x)\right\}\right] \tag{15}$$

where k_c and k_a are the rate constants of the cathodic and anodic reactions, respectively.

As the partial pressure distributions and current distribution in the electrolyte have been obtained, distributions of the activation overpotentials $\eta_c(x)$ and $\eta_a(x)$ can be calculated using Eqs. (14) and (15). Moreover, by subtracting the anode and cathode activation overpotentials from electromotive force as expressed in Eq. (16), we can obtain net electromotive force distribution $\mathrm{emf}^*(x)$.

$$\mathrm{emf}^*(x) = \mathrm{emf}(x) - \{|\eta_c(x)| + \eta_a(x)\} \tag{16}$$

Eq. (4) can be solved again using this new $\mathrm{emf}^*(x)$, and then the new distributions of current, concentration, partial pressure, emf and activation overpotential can be obtained. These calculations are iterated until convergence is achieved. After the convergence is achieved, if the IR drops along current path is subtracted from $\mathrm{emf}^*(x)$, cell voltage at given cell current $V(I_0)$ can be obtained [3].

$$V(I_0) = \mathrm{emf}^*(x) - \{\eta_{IR,a}(x) + \eta_{IR,e}(x) + \eta_{IR,c}(x)\} \tag{17}$$

where $\eta_{IR,a}(x)$, $\eta_{IR,e}(x)$ and $\eta_{IR,c}(x)$ are IR drops in the anode, electrolyte and cathode, respectively.

2.5. Energy losses

In the equivalent circuit described in Fig. 3, the energy losses for the activation overpotentials $E_{\mathrm{loss,act}}$, for the IR drop in the electrodes $E_{\mathrm{loss,el}}$ and for the IR drop in the electrolyte $E_{\mathrm{loss,ion}}$ are expressed by following equations:

$$E_{\mathrm{loss,act}} = \int_0^L I_e(x)\{|\eta_c(x)| + \eta_a(x)\}\mathrm{d}x \tag{18}$$

$$E_{\mathrm{loss,el}} = \int_0^L I_a^2(x)\frac{\rho_a(x)}{t_a W}\mathrm{d}x + \int_0^L I_c^2(x)\frac{\rho_c(x)}{t_c W}\mathrm{d}x \tag{19}$$

$$E_{\mathrm{loss,ion}} = \int_0^L I_e^2(x)\rho_e(x)\frac{d}{W}\mathrm{d}x \tag{20}$$

2.6. Energy conversion efficiency

Theoretical thermal efficiency of fuel cell $\varepsilon_{\mathrm{th}}$ is given by:

$$\varepsilon_{\mathrm{th}} = \frac{\Delta G^\circ(T)}{\Delta H^\circ(298\,\mathrm{K})} \times 100 \tag{21}$$

where $\Delta G^\circ(T)$ is standard Gibbs energy change of hydrogen combustion at T K and $\Delta H^\circ(298\,\mathrm{K})$ is lower-heating value (LHV) of hydrogen combustion.

Energy conversion efficiency of fuel cell system, ε_s can be expressed by:

$$\varepsilon_s = \frac{I_0 V_t(I_0)}{M_{\mathrm{H_2}}(0)\,\Delta H^\circ(298\,\mathrm{K})} \times 100 \tag{22}$$

where $V_t(I_0)$ is total cell voltage of planar stack fuel cell. On the other hand, energy conversion efficiency from chemical energy to electricity ε_e can be expressed by following equation:

$$\varepsilon_e = \frac{I_0 V_t(I_0)}{U_{\mathrm{H_2}} M_{\mathrm{H_2}}(0)\,\Delta H^\circ(298\,\mathrm{K})} \times 100 \tag{23}$$

2.7. Calculation of the output power for planar stack fuel cells

As shown in Fig. 4, in the planar stack fuel cell, single cell is divided into several segments and they are placed in the direction of the gas flow. The number of segments is denoted by N and each cell is written by segment number n. In the five segments cell, $n = 1$ denotes first segment cell namely gas inlet side cell, on the other hand $n = 5$ denotes fifth segment cell, namely, gas outlet side cell. For the simplification, interconnection and the effects of the mixing of the cathode and anode side gases in the gap between the neighbor cells are neglected. First, I–V curve for the first segment is calculated by above mentioned procedure and the values of partial pressures at gas exit of the first segment are obtained for a given load current I_0. Then, I–V curve for the second segment cell can be calculated by the same procedure using these partial pressure values. The total cell voltage and

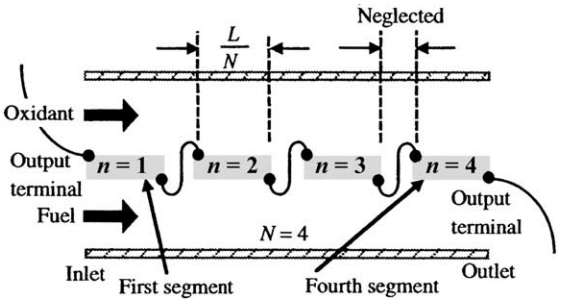

Fig. 4. Configuration of the planar stack fuel cell.

electric power for a planar stack SOFC are obtained as the sum of the values of all segments.

The total cell length and cell width, L and W, are fixed at 3 and 1 cm because these dimensions are suitable for portable electric devices, and N is varied from 1 to 5. The structural parameters and operating conditions are summarized in Table 1. The conditions of Table 1 are based on the experimental conditions in the measurement of the discharge characteristics of single chamber SOFC reported by Hibino et al. [7].

3. Results and discussion

U_{H_2} is introduced as an operating condition in place of cell current I_0, because this parameter is more useful than I_0 to compare the discharge properties of single cell and planar stack cell. U_{H_2} is expressed as:

$$U_{H_2} = \frac{NI_0}{2FM_{H_2,f}(0)} \tag{24}$$

The relationship between U_{H_2} and I_0 at present conditions is shown in Fig. 5. Cell current in the N segments cell becomes $1/N$ of single cell. However, current density

Table 1
Values used in the calculation

Structural parameters	
Cell width, W (cm)	1
Cathode thickness, t_c (cm)	0.0017
Anode thickness, t_a (cm)	0.0017
Electrolyte thickness, d (cm)	0.05
Operating conditions	
Temperature, T (K)	1223
Oxygen partial pressure at oxidant inlet, $P_{O_2}(0)$ (atm)	0.165
Hydrogen partial pressure at fuel inlet, $P_{H_2}(0)$ (atm)	0.082
Water vapor partial pressure at fuel inlet, $P_{H_2O}(0)$ (atm)	0.058
Flow rate of inlet gases, f ($cm^{-3}\ s^{-1}$)	2.5
Other parameters	
Resistivity of LSM, ρ_c (Ω cm)	0.0083
Resistivity of Ni, ρ_a (Ω cm)	0.001
Resistivity of YSZ, ρ_e (Ω cm)	13.8
Rate constant for the cathodic reaction, k_c (A cm^{-2})	0.218
Rate constant for the anodic reaction, k_a (A cm^{-2})	0.427

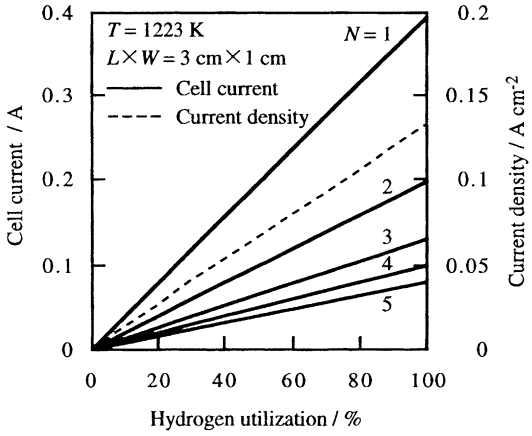

Fig. 5. Relationship between hydrogen utilization and cell current applied in planar stack SOFC. Calculation conditions are equal to Table 1.

expressed with $I_0/(LW/N)$ (dotted line) is determined by U_{H_2} independently of the number of segmented cells.

3.1. Output power

Fig. 6 shows the relationship between hydrogen utilization and output power of planar stack SOFC calculated using the model of Fig. 3. It is obvious that single cell with length of 3 cm generates only 50 mW at the most. However, output power of SOFC remarkably increases by dividing a single cell into segment cells in the gas flow direction. In the five segments cell, more than 200 mW can be generated at $U_{H_2} = 80\%$ (105 mA cm^{-2}). This value is considered to be useful for portable electric devices. These results are summarized in Table 2. In the following section, the reason for the output power increase by cell partition will be discussed from the viewpoint of energy losses.

3.2. Energy losses

Fig. 7 shows the energy losses for the activation overpotentials $E_{loss,\ act}$, IR drop in the electrolyte $E_{loss,\ ion}$ and IR

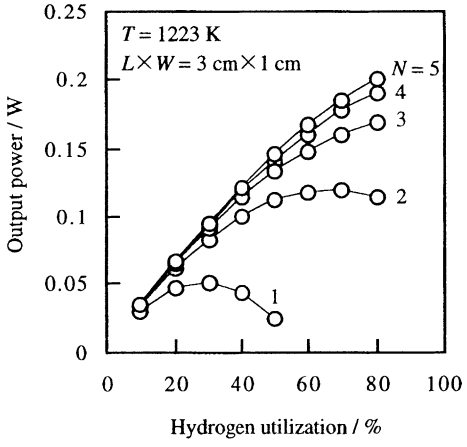

Fig. 6. Output power of planar stack SOFC for various segment numbers.

Table 2
Dependence of discharge characteristics of planar stack SOFC on the number of segment cells for isothermal case

	Output power (mW)		$E_{loss,\ el}$ (mW)		$E_{loss,\ ion}$ (mW)		$E_{loss,\ act}$ (mW)		ε_s (%)	
	$U_{H_2} = 50\%$	$U_{H_2} = 80\%$	$U_{H_2} = 50\%$	$U_{H_2} = 80\%$	$U_{H_2} = 50\%$	$U_{H_2} = 80\%$	$U_{H_2} = 50\%$	$U_{H_2} = 80\%$	$U_{H_2} = 50\%$	$U_{H_2} = 80\%$
Single SOFC										
$N = 1$	23		102		25		20		4.9	
Planar stack SOFC										
$N = 2$	112	114	34	87	13	35	12	30	23	23
$N = 3$	133	168	18	46	11	27	9.5	25	27	34
$N = 4$	142	190	11	29	9.6	25	8.7	23	29	38
$N = 5$	146	201	7.7	20	9.3	24	8.4	22	30	41

drop in the electrodes $E_{loss,\ el}$, respectively. As seen in this figure, since current must be applied to thin electrode layers, terrible energy loss takes place in the electrodes of single cell due to excessively long length in the current flow direction. In the present conditions, $E_{loss,\ el}$ is considerably larger than $E_{loss,\ act}$ and $E_{loss,\ ion}$ when the number of segment cells are less than 3, however, in the five segments cell $E_{loss,\ el}$ becomes smaller than the other energy losses. Fig. 8 shows the relationship between cell current I_0 and $E_{loss,\ el}$ for

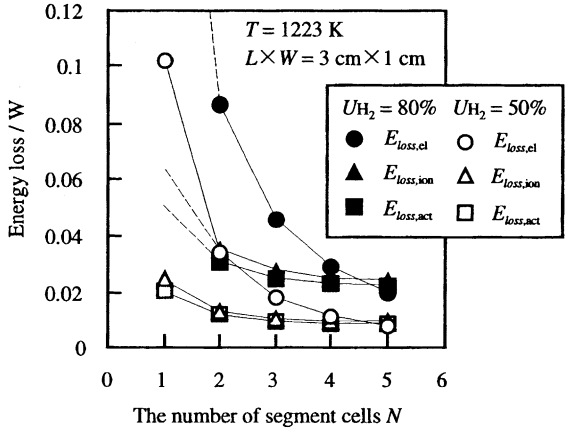

Fig. 7. Dependence of energy losses in the planar stack SOFC on the number of segment cells.

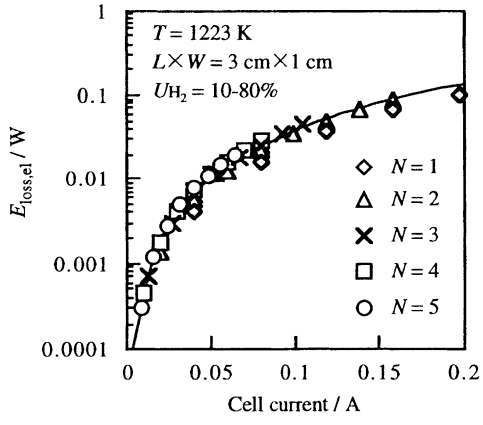

Fig. 8. Relationship between cell current applied in planar stack SOFC and energy loss caused by *IR* drop in the both electrodes.

various segment numbers N. It is clear that $E_{loss,\ el}$ in planar stack SOFC is approximately determined by load current I_0. Then, because cell current of planar stack SOFC becomes $1/N$ of single cell at a same U_{H_2} as shown in Fig. 5, $E_{loss,\ el}$ can be dramatically reduced by increasing the number of segment cells N. On the other hand, as shown in Fig. 7, $E_{loss,\ act}$ and $E_{loss,\ ion}$ can also be reduced by increasing N. As can be seen in Fig. 9(a), in the single cell, current in the electrolyte significantly increases near the gas inlet side for the following two reasons. First is the difference in fuel concentration between gas inlet and outlet. As shown in Fig. 10(a), fuel concentration decreases towards downstream, therefore, emf(x) decreases along gas flow direction. This results in current concentration at gas inlet side due to highest driving force for electrochemical reaction. This effect is considered at the third term in the right side of Eq. (2). Second is the difference in electrode resistances between cathode and anode. This effect corresponds to the first and second terms

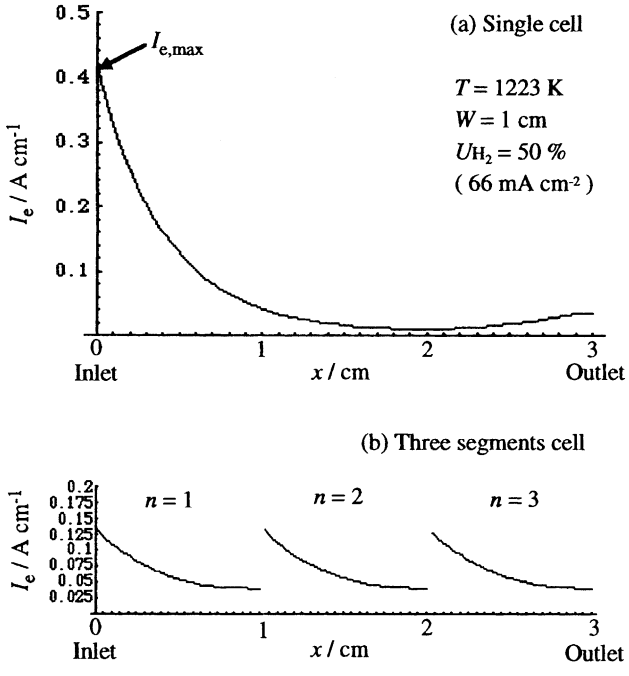

Fig. 9. Distribution of current in the electrolyte at $U_{H_2} = 50\%$: (a) for the single SOFC and (b) for the planar stack SOFC (three segments cell).

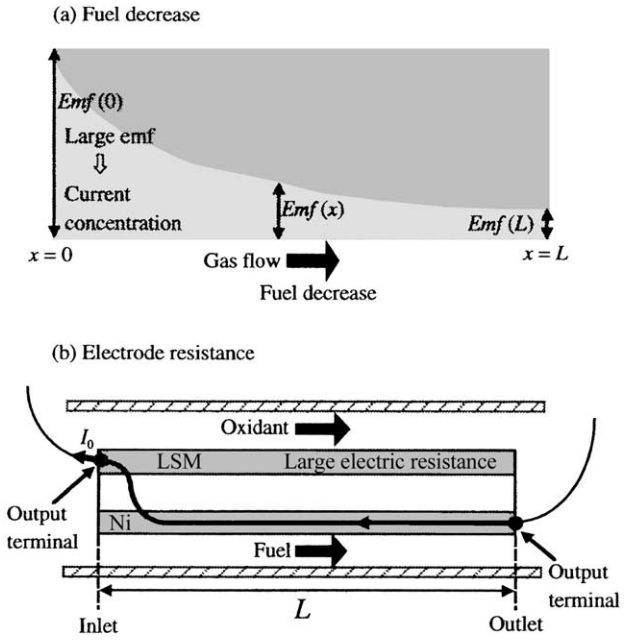

Fig. 10. Increase in current in the electrolyte near the gas inlet side.

in the right side of Eq. (2). When the cathode and anode resistances do not agree with each other, cell current will pass in favor of in the electrode that has lower resistance. At present conditions, LSM has about 10 times as large resistance as Ni has. Therefore, current passes mainly in Ni as shown in Fig. 10(b). This is the main cause of current localization at gas inlet side. Naturally, current concentration observed in Fig. 9(a) gives rise to activation overpotential increase nearby the gas inlet side on both the electrodes. Concentrations of current and activation overpotential at gas inlet side are the reasons why $E_{\text{loss, act}}$ and $E_{\text{loss, ion}}$ of the single cell become large as seen in Fig. 7. However it is clear that these energy losses decrease with increasing N, because as shown in Fig. 9(b) current in the electrolyte becomes more uniform by dividing a single cell into segments. Current concentration in the electrolyte is defined as the ratio of maximum current $I_{\text{e, max}}$ to average current $I_{\text{e, ave}}$. By the way, according to Eq. (2), if the resistance parameters of cathode and anode, $R_c(x)$ and $R_a(x)$, are set at 0, we can obtain current distribution in the electrolyte caused by fuel decrease in the gas flow direction, therefore current concentration due to fuel distribution also can be estimated. The relationship between the number of segment cells and current concentration is shown in Fig. 11. As for planar stack SOFC, $I_{\text{e, max}}$ is the average value of that in each segment cell. As observed in Fig. 11, the current concentration decreases with increasing N with the relation of $I_{\text{e, max}}/I_{\text{e, ave}} = 6.0N^{-0.9}$, and it is clear that current concentration in the electrolyte of the single cell is caused by mainly the difference in electric resistance between cathode and anode. For the single cell, 80% of the current concentration is due to the difference in the electric resistances. In contrast, for the five segments cell, 80% of

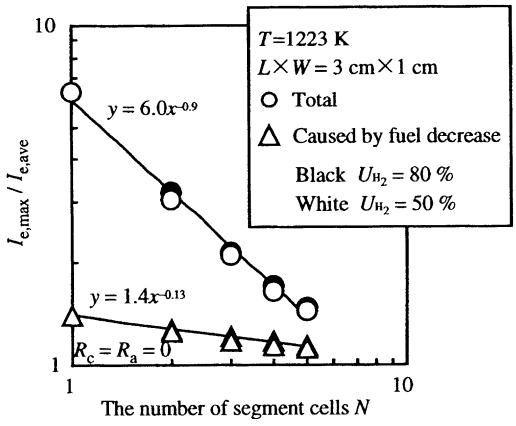

Fig. 11. The effect of the number of segment cells on current concentration in the electrolyte.

that is due to the fuel decrease in the gas flow direction. Dependence of $E_{\text{loss, act}}$ and $E_{\text{loss, ion}}$ on the current concentration is shown in Fig. 12. As can be seen in Fig. 12, by increasing N, at a same hydrogen utilization or current density, $E_{\text{loss, act}}$ and $E_{\text{loss, ion}}$ can be reduced depending on the decrease of the current concentration in the electrolyte, and the change of the energy loss value $\Delta\log E_{\text{loss}}$ is determined by the change of the current concentration $\Delta(I_{\text{e, max}}/I_{\text{e, ave}})$. These reductions of energy losses by cell partition correspond to the output power increase shown in Fig. 6. The dependence of energy losses on the number of segment cells is also summarized in Table 2.

3.3. Energy conversion efficiency

Dependence of energy conversion efficiency on the number of segment cells is shown in Fig. 13. The ε_s is very small when N is equal to 1 because of large IR drop in the electrodes and its maximum value is about 10% when U_{H_2} is 30 %. However, if N and U_{H_2} are increased up to 5 and 80%, respectively, system efficiency increases up to

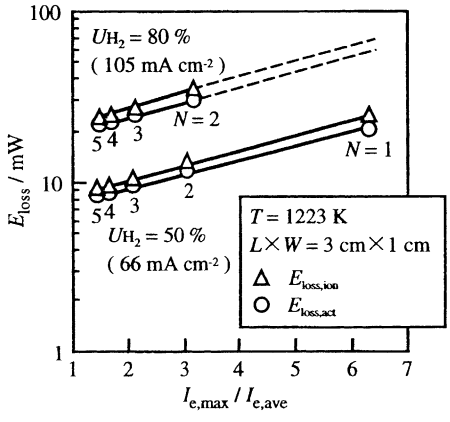

Fig. 12. Dependence of energy losses caused by activation overpotentials $E_{\text{loss, act}}$ and IR drop in the electrolyte $E_{\text{loss, ion}}$ on the current concentration.

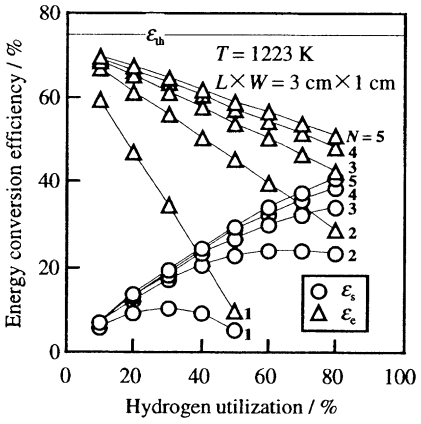

Fig. 13. Energy conversion efficiency of planar stack SOFC for various segment numbers.

around 40%. On the other hand, ε_e increases up to near the theoretical value by decreasing U_{H_2} down to near 0%. Especially in the five segments cell, ε_e is 70–50% in the U_{H_2} range from 10 to 80%. Fig. 13 shows that cell partition which leads to remarkable reduction of energy losses as discussed in Section 3.2 is an effective way of fuel cell efficiency increasing.

4. Conclusions

The configuration of planar stack fuel cell is most promising design for portable electric devices, however so far its discharge characteristics have not been analyzed quantitatively. Therefore, prior to fabrication of this fuel cell system, it is very important to clarify its discharge characteristics using mathematical model. In order to analyze the properties of planar stack fuel cell in SOFC field, Mathematica™ program to calculate *I–V* curve of planar stack SOFC taking electric resistances of component materials and activation overpotentials into consideration has been made.

Single cell of small size SOFC can not generate sufficient electric power to run portable electric devices. However, output power can be increased at a certain hydrogen utilization by dividing a single cell into segment cells along gas flow direction, in other words, employing planar stack configuration because energy losses for the *IR* drops in both the electrodes, *IR* drop in the electrolyte and the activation overpotentials can be considerably reduced by cell partition. In particular, energy losses for *IR* drop in the electrolyte and the activation overpotentials are closely related to current concentration in the electrolyte, and the reduction of current concentration by cell partition is one of the reasons for high electric power of planar stack SOFC.

Only hydrogen/oxygen separate system was considered in this paper for simplification. But the dealt system is not suitable for the electric power source of portable electronics in the points of operating temperature and considered fuel. The one-chamber SOFC developed by Hibino et al. which can be operated at low temperatures below 773 K [8] is most promising system in the view of portable applications. In the SOFC field, the planar stack configuration will become more effective for practical applications, especially when it is incorporated into the one-chamber fuel cells because of no need of separators (Fig. 1).

References

[1] Y. Shiratori, Y. Yamazaki, Electrochemistry 69 (2001) 92–97.
[2] J. Newman, Electrochemical Systems, Corona sha, Tokyo, 1973, pp. 375–377 (in Japanese).
[3] S. Nagata, K. Shirai, H. Sato, Bull. Electrotechnol. Lab. 40 (1976) 974–987.
[4] S. Nagata, Y. Kaga, Y. Kasuga, H. Sato, Y. Ohno, Trans. Inst. Elect. Eng. Jpn. 107 B (1987) 147–154.
[5] S. Nagata, Y. Kasuga, Trans. Inst. Elect. Eng. Jpn. 112 B (1992) 267–275.
[6] Da.Yu. Wang, A.S. Nowick, J. Electrochem. Soc. 126 (1979) 1155–1165.
[7] T. Hibino, S. Wang, S. Kakimoto, M. Sano, Solid State Ionics 127 (2000) 89–98.
[8] T. Hibino, A. Hashimoto, T. Inoue, J. Tokuno, S. Yoshida, M. Sano, Science 288 (2000) 2031–2033.